PHYSICAL REVIEW B **91**, 134301 (2015)

Heat-flux control and solid-state cooling by regulating chemical potential of photons in near-field electromagnetic heat transfer

Kaifeng Chen,[1] Parthiban Santhanam,[2] Sunil Sandhu,[2] Linxiao Zhu,[1] and Shanhui Fan[2,*]

[1]*Department of Applied Physics, Stanford University, California 94305, USA*

[2]*Department of Electrical Engineering, Ginzton Laboratory, Stanford University, Stanford, California 94305, USA*

(Received 1 October 2014; revised manuscript received 28 January 2015; published 13 April 2015)

We consider near-field heat transfer with nonzero chemical potential for photons, as can occur between two semiconductor bodies, held at different temperatures with at least one of the bodies under external bias. We show that the dependence of radiative heat flux on chemical potential enables electronic control of both the direction and magnitude of near-field heat transfer between the two bodies. Moreover such a configuration can operate as a solid-state cooling device whose efficiency can approach the Carnot limit in the ideal case. Significant cooling can also be achieved in the presence of inherent nonidealities including Auger recombination and parasitic phonon-polariton heat transfer.

DOI: 10.1103/PhysRevB.91.134301 PACS number(s): 44.40.+a

I. INTRODUCTION

Near-field electromagnetic heat transfer through vacuum has been of fundamental importance because the power density of the energy flow can be enhanced beyond Planck's law of blackbody radiation [1–3]. In recent years, such enhancement has been demonstrated experimentally [4–8]. Theoretical explorations of increasingly complex geometries are widely discussed [9–18]. Moreover, there has been growing interest in active control of near-field heat transfer [19–29].

In all previous works on near-field heat transfer between two bodies, one assumes a zero chemical potential for the objects involved. However, photons can have a chemical potential when they are in quasiequilibrium with a semiconductor under external bias [30]. Yet the consequences of such nonzero chemical potential for near-field heat transfer have not been explored previously. In this paper, based on the fluctuational electrodynamics formalism, we provide a direct calculation of near-field heat transfer between two bodies, each taken to be in quasiequilibrium, in the presence of a nonzero chemical potential. We show that the use of such chemical potential enables electronic control of near-field heat transfer.

Furthermore, when considering heat transfer between cold and hot objects, applying a chemical potential on the cold object can result in a net heat flow from the cold to the hot object, and hence the resulting structure can be used for cooling purposes. Therefore, near-field heat transfer in the presence of nonzero chemical potential provides an important, previously unexplored mechanism for solid-state cooling. We show that in the ideal limit, such a cooling device can have an efficiency that approaches the Carnot efficiency. We also consider the effect of intrinsic nonidealities, including nonradiative Auger recombination and parasitic heat transfer through surface phonon polaritons. We show that the structure can still provide cooling with reasonable efficiency, in spite of these nonidealities, with a heterostructure design consisting of two different semiconductors.

The paper is organized as follows. In Sec. II, we present the configuration and the formalism. In Sec. III, we discuss the ideal case and show that the numerical results can be well explained by a simple analytical model. In Sec. IV, we consider the effect of nonidealities. We summarize and conclude in Sec. V.

II. THE CONFIGURATION AND FORMALISM

A. The configuration

Throughout the paper, we consider the configuration in Fig. 1, where two intrinsic semiconductors, labeled bodies 1 and 2, with thickness t_1 and t_2, respectively, are brought into close proximity with a vacuum gap separation d. The temperatures of the two bodies are labeled T_1 and T_2 ($T_1 < T_2$), respectively. To control the chemical potential of each semiconductor, we assume that the back side of each intrinsic semiconductor region forms a junction with a small heavily doped p^+ or n^+ region, which then connects to external contacts. For each body, assuming perfect contacts, the quasi-Fermi level of the electrons in the intrinsic region is set by the potential at the n-type contact while that of the holes is set by the p-type contact. Taking the body to be optically thick for photons with frequencies above the band gap energy, the resulting nonequilibrium state of the electron-hole system gives rise to an outgoing photon field from interband transitions with a chemical potential qV [30–32]. For simplicity, we apply zero voltage to body 2, i.e., we short body 2 for the calculations in this paper.

Intuitively, when compared to the case without applied voltage, one should expect increased photon emission from body 1 as one applies a forward-bias voltage on it. Thus, the near-field heat transfer between the two bodies can be influenced by the applied voltage. Moreover, in the case where body 1 is colder than body 2, such an increased photon emission may nevertheless result in a net heat flow from body 1 to body 2. Hence by using electrical work as delivered by an applied voltage, one could pump heat from a cold body to a hot body. The objective of this paper is to study such electronically controlled heat transfer in detail, and to evaluate its performance as a solid-state cooling device.

*shanhui@stanford.edu

 ©2015 American Physical Society

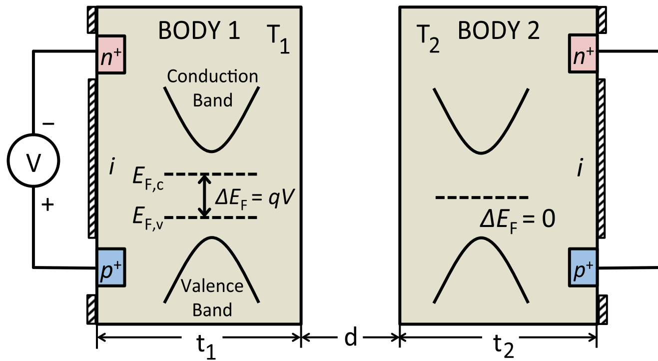

FIG. 1. (Color online) Schematic of the configuration. The system consists of two bodies, i.e., body 1 and body 2, separated by a small distance d which is much smaller than their extent in the dimensions transverse to the gap. The two-body structure is enclosed within perfect mirrors at the extreme left and right boundaries. Depictions of the relevant bands and the corresponding quasi-Fermi levels of the two semiconductors are also included in the figure. With an external forward bias V applied to body 1, the quasi-Fermi levels for its electrons and holes are separated by $\Delta E_F = qV$. Body 2 is electrically shorted so it has $\Delta E_F = 0$. Throughout the paper, we choose $T_1 = 290$ K, $T_2 = 300$ K.

B. Dielectric function and current fluctuations of semiconductors under external bias

We study the system shown in Fig. 1 using the the formalism of fluctuational electrodynamics [33]. In this formalism, one describes the heat transfer between objects by computing the electromagnetic flux resulting from fluctuating current sources inside each object. The magnitude of the current fluctuation is related to the imaginary part of the dielectric function of the object. Therefore, we start with a brief discussion of the dielectric function and the corresponding current fluctuation of a semiconductor under external bias. Since we will primarily be considering a temperature range near the room temperature, we will consider the narrow-band gap semiconductors [34,35] such as InAs and InSb whose band gaps are 0.354 and 0.17 eV at room temperature, respectively.

The dielectric function of such III-V semiconductors has contributions from both interband electronic transitions at frequencies above the band gap and from phonon-polariton excitations at frequencies well below the band gap. We denote the contributions to the dielectric function from the electronic transitions and the phonon-polariton excitations as $\epsilon_e(\omega,V)$ and $\epsilon_p(\omega)$, respectively. The overall dielectric function has contributions from these two processes:

$$\epsilon(\omega,V) = \begin{cases} \epsilon_e(\omega,V) & (\omega \geqslant \omega_c) \\ \epsilon_p(\omega) & (\omega < \omega_c), \end{cases} \quad (1)$$

where ω_c is the cut-off frequency between interband electronic transitions and phonon-polariton excitations. In our calculations, we choose ω_c to be somewhat below the electronic band gap frequency where the imaginary part of the dielectric function is near zero.

For narrow-band-gap semiconductors, a forward bias will easily shift the quasi-Fermi levels towards the degenerate regime where the Boltzmann approximation of electron occupation fails. This will result in a significant change in the imaginary part of $\epsilon_e(\omega,V)$, denoted as $\epsilon_e''(\omega,V)$, as a function of external bias. For degenerate semiconductors, it is known that $\epsilon_e''(\omega,V)$ is related to V only through $\bar{n}_\mathrm{v} - \bar{n}_\mathrm{c}$. Here $\bar{n}_\mathrm{c}$ and $\bar{n}_\mathrm{v}$ are the average occupation numbers for the conduction band edge states and valence band states, respectively, that satisfy the vertical transition condition at the frequency ω [31]. Therefore

$$\epsilon_e''(\omega,V) = \frac{(\bar{n}_\mathrm{v} - \bar{n}_\mathrm{c})}{(\bar{n}_\mathrm{v} - \bar{n}_\mathrm{c})|_{V=0}}\, \epsilon_e''(\omega,0). \quad (2)$$

As we vary the voltage, the change in the real part of $\epsilon_e(\omega,V)$ is generally quite small, and is therefore ignored in our calculations.

In the presence of external bias, photons emitted from interband transitions can carry a nonzero chemical potential [30]. Consider a semiconductor whose electronic degrees of freedom (i.e., its electrons and holes) are excited by an external voltage V, maintained at a temperature T. The quasi-Fermi levels of the electrons and holes are separated by qV, where q is the magnitude of the electron's charge. A photon gas in equilibrium with such a semiconductor through electronic interband transitions then satisfies the Bose-Einstein distribution

$$\Theta(\omega,T,V) = \frac{\hbar\omega}{\exp\left(\frac{\hbar\omega - qV}{k_B T}\right) - 1}, \quad (3)$$

where $\Theta(\omega,T,V)$ is the expectation value of photon energy in a single mode at angular frequency ω, $\hbar$ is the reduced Planck constant, and k_B is the Boltzmann constant. In Eq. (3), qV plays the role of chemical potential for photons. Using the fluctuation-dissipation theorem, the thermal electromagnetic fields as generated by interband transitions can then be described by random thermal current sources $j_\alpha(\boldsymbol{r},\omega)$ in the semiconductor with the correlation function [31]

$$\langle j_\alpha(\boldsymbol{r},\omega) j_\beta^*(\boldsymbol{r}',\omega')\rangle_e = \frac{4}{\pi}\omega\, \Theta(\omega,T,V)\, \delta(\boldsymbol{r}-\boldsymbol{r}')\, \delta(\omega-\omega')\, \epsilon_e''(\omega,V)\, \delta_{\alpha\beta}, \quad (4)$$

where α and β label the directions of polarization, $\boldsymbol{r}$ and $\boldsymbol{r}'$ are position vectors, and $\delta(\omega-\omega')$ is the Dirac delta function. This expression is derived in Ref. [31] using linear response theory and Kubo's formula. The derivation assumes that the electromagnetic fields are weak. In practice, Eq. (4) is valid when $\frac{E_g - qV}{k_B T} \gg 1$, and hence the system is in the spontaneous emission regime. Equation (4) is no longer applicable when the applied voltage V is comparable or even greater than E_g/q, in which case strong stimulated emission or even lasing can occur and the weak-field assumption is no longer valid.

In addition to the electronic transition, III-V semiconductors also can couple electromagnetically via polaritons with angular frequencies corresponding to their polar optical phonon bands. The bulk phonon-polariton energies for InAs and InSb are 0.0276 [36] and 0.025 eV [37], respectively. As we will see, the presence of these phonon polaritons also contributes significantly to the energy transfer between the semiconductors. The imaginary part of the dielectric function in this frequency range is denoted as $\epsilon_p''(\omega)$ and is independent of external bias. Using the fluctuation-dissipation theorem, the correlation function of the random sources due

to phonon-polariton excitations is then

$$\langle j_\alpha(\boldsymbol{r},\omega) j_\beta^*(\boldsymbol{r}',\omega')\rangle_p = \frac{4}{\pi}\omega\,\Theta(\omega,T,0)\,\delta(\boldsymbol{r}-\boldsymbol{r}')\,\delta(\omega-\omega')\,\epsilon_p''(\omega)\,\delta_{\alpha\beta}. \quad (5)$$

Unlike the random current sources corresponding to electronic interband transition in Eq. (4), here the magnitude of the fluctuation is independent of the external voltage. Combining Eqs. (4) and (5) allows us to treat the electromagnetic near-field heat transfer between semiconductors under external bias, taking into account the intrinsic dissipation mechanisms of these materials. Note that the phonon-polariton frequencies are far below the band-gap frequencies, which justifies the separate treatment of electronic transitions and phonon-polariton excitations in Eq. (1).

C. Electromagnetic formalism

We use the standard dyadic Green's function [12,13] technique to compute the transferred power density from the current fluctuation [1] presented in Sec. II B. Details on the dyadic Green's function can be found in Ref [38]. We compute separately the two nonoverlapping emitted photon energy flux spectra $\Phi_e(\omega)$ and $\Phi_p(\omega)$ [39] associated with photons emitted from above-band-gap electronic transitions and phonon-polariton excitations, respectively. The energy fluxes E^e and E^p, for above- and below-band-gap photons, respectively, are then obtained by integration over the appropriate frequency ranges

$$E^e_{a\to b} = \int_{\omega_c}^{+\infty} \Theta(\omega,T_a,V_a)\Phi_e(\omega)\,d\omega, \quad (6)$$

$$E^p_{a\to b} = \int_0^{\omega_c} \Theta(\omega,T_a,0)\Phi_p(\omega)\,d\omega. \quad (7)$$

The subscripts (a,b) in Eqs. (6) and (7) can be either (1,2) or (2,1) depending on the flux direction (Fig. 1). In Eqs. (6) and (7), ω_c is as defined in Eq. (1). We attribute the transfer at frequencies above this frequency to interband electronic transition and below it to phonon-polariton excitations, respectively. The overall heat transfer between the two bodies is

$$E_{a\to b} = E^e_{a\to b} + E^p_{a\to b}. \quad (8)$$

A similar calculation also yields the above-band-gap photon flux between the two bodies as

$$F_{a\to b} = \int_{\omega_c}^{+\infty} \frac{\Theta(\omega,T_a,V_a)}{\hbar\omega}\Phi_e(\omega)\,d\omega. \quad (9)$$

For later use, we define

$$F^0_{a\to b} = F_{a\to b}|_{V_a=0}. \quad (10)$$

D. Detailed balance relations

The formalism described in Sec. II C enables us to compute the dependence of heat power transfer rate as a function of applied voltage. In order to further evaluate the performance of such a configuration for cooling purposes, we need to calculate the injected electric power density into body 1. This electric power density is just the product of the external bias V and the injected current density J to body 1. By detailed balance, the current density J must be related to the total recombination rate as

$$J = q\,(F_{1\to 2} - F_{2\to 1} + R), \quad (11)$$

where $F_{1\to 2}$ and $F_{2\to 1}$ are defined in Eq. (9). $(F_{1\to 2} - F_{2\to 1})$ and R represent the net radiative recombination rate and nonradiative rate, respectively, per unit area in body 1. In this paper, for nonradiative recombination, we consider only the Auger process, which is intrinsic and dominates in high-quality materials. Because of our short circuit condition on body 2, the computations in this paper will require considering the Auger process only in InAs. Here we set R in Eq. (11) to [40]

$$R = (C_n n + C_p p)\left(np - n_i^2\right) t_1, \quad (12)$$

where n and p are the electron and hole concentrations, respectively, and t_1 is the thickness of body 1. At 290 K, for InAs, $C_0 = C_p + C_n = 2.26\times 10^{-27}$ cm^6 s^{-1} is the Auger recombination coefficient (the value of C_0 is computed from its value at 300 K as shown in [41], taking into account the temperature dependence of C_0 [42]). $n_i = 6.06\times 10^{14}$ cm^{-3} is the intrinsic carrier concentration at 290 K. Having computed the injected current into body 1, we then obtain the net outflow power density from body 1:

$$P = (E_{1\to 2} - E_{2\to 1}) - JV. \quad (13)$$

III. IDEAL CASE

Using the formalism in Sec. II, we now consider the heat transfer in the configuration shown in Fig. 1, when an external bias voltage is applied to body 1. In this section, we first consider the ideal case, where we ignore the contributions from nonradiative recombination [$R = 0$ in Eq. (11)] and phonon-polariton excitations [$E^p_{a\to b} = 0$ in Eq. (8)]. In such an ideal case, we introduce an analytical model for heat transfer, first in Sec. III A for the *homojunction* structure where the two semiconductors are the same, and then in Sec. III B for the *heterojunction* structure where the two semiconductors are different. For both structures, the analytical model predicts an exponential dependence of the heat transfer power as a function of voltage. The model also predicts that in the ideal case the efficiency of this configuration as a cooling device can approach the Carnot limit. We show in Sec. III C that the prediction of such an analytical model agrees very well with direct computations based on the fluctuational electrodynamics formalism.

A. Analytical model for homojunction structure

We consider the homojunction structure first. In our model, we assume

$$\exp\left(\frac{\hbar\omega_g - qV}{k_B T}\right) \gg 1. \quad (14)$$

Under this condition, the emission spectra of the semiconductors are strongly peaked near the band-gap frequency ω_g of the semiconductor. Thus from Eq. (9) we have the photon flux

$$F_{1\to 2} = \exp\left(\frac{qV}{k_B T_1}\right) F^0_{1\to 2}. \quad (15)$$

Furthermore, Eq. (6) can be simplified as

$$E^{e}_{1\to 2} = \exp\left(\frac{qV}{k_B T_1}\right) \hbar\omega_g F^0_{1\to 2}, \tag{16}$$

$$E^{e}_{2\to 1} = \hbar\omega_g F^0_{2\to 1}. \tag{17}$$

Therefore, we see that the transferred power has an exponential dependency on the applied voltage.

We now consider the cooling performance of this configuration. From Eqs. (9) and (11), the current density in body 1 in the presence of external voltage V is

$$J = q\left(e^{qV/k_B T_1} F^0_{1\to 2} - F^0_{2\to 1}\right). \tag{18}$$

Using Eq. (13) and combining it with Eqs. (16)–(18), the net outflow power density from body 1 is then

$$P = \left(e^{qV/k_B T_1} F^0_{1\to 2} - F^0_{2\to 1}\right)(\hbar\omega_g - qV). \tag{19}$$

For cooling purposes, one sets $T_1 < T_2$. In the absence of external voltage, $F^0_{1\to 2} < F^0_{2\to 1}$, i.e., there is a net inflow of power to the cold body 1, as required by the second law of thermodynamics. With the application of voltage, however, there is an exponential increase of the radiative power from body 1. As a result, P in Eq. (19) may change sign, indicating a net outflow of power from the cold body 1 to the hot body 2 and hence the possibility of cooling.

The voltage where $P = 0$ defines the threshold voltage V_t. In this model, the condition of $P = 0$ coincides with $J = 0$ at the threshold voltage V_t. Therefore, based on Eqs. (6) and (13) we have

$$\Theta(\omega_g, T_1, V_t) = \Theta(\omega_g, T_2, 0), \tag{20}$$

from which we obtain

$$V_t = \frac{\hbar\omega_g}{q}\frac{T_2 - T_1}{T_2}. \tag{21}$$

For a cooling device, the standard metric for its efficiency is the *cooling coefficient of performance* (COP) [43] defined as

$$\mathrm{COP} = \frac{P}{JV}, \tag{22}$$

where P [in Eq. (13)] measures the net outflow of heat from the cold body, and JV is the injected electric power into body 1. Substituting Eqs. (18) and (19) into Eq. (22) results in

$$\mathrm{COP} = \frac{\left(e^{qV/k_B T_1} F^0_{1\to 2} - F^0_{2\to 1}\right)(\hbar\omega_g - qV)}{\left(e^{qV/k_B T_1} F^0_{1\to 2} - F^0_{2\to 1}\right) qV} = \frac{\hbar\omega_g}{qV} - 1. \tag{23}$$

According to the second law of thermodynamics, the COP should be bounded by the *Carnot limit*, i.e.,

$$\mathrm{COP} \leqslant \frac{T_1}{T_2 - T_1}. \tag{24}$$

From Eqs. (21) and (23), we see that the COP reaches the Carnot limit at $V = V_t$, and falls below the Carnot limit when $V > V_t$. At Carnot limit, the net cooling power density approaches zero. Thus, for most practical applications one would not operate at the Carnot limit even if the device is capable of achieving this limit.

B. Analytical model for heterojunction structure

The simple analytical model in Sec. III A for the homojunction structure can be straightforwardly generalized to the heterojunction structure where the two semiconductors have different band gaps. Without loss of generality, we assume that the two semiconductors have band-gap frequencies ω_{g1} and ω_{g2}, respectively, with $\omega_{g1} > \omega_{g2}$. The thermal exchange between the semiconductors will only occur in the frequency range above ω_{g1}. Thus, from the results in Sec. III A, we can replace ω_g by ω_{g1} to obtain the corresponding results for the heterojunction case, which reaches the Carnot limit at $V = V_t$ as well.

For cooling purposes, the semiconductor on the cold side should have a band gap that is larger as compared to the semiconductor on the hot side to ensure that all the emission from the cold side can be absorbed by the hot side.

C. Numerical results

To directly check the analytical model, we performed exact calculations based on fluctuational electrodynamics. We consider the configuration in Fig. 1 and set the temperatures for the hot and cold bodies to be $T_1 = 290$ K and $T_2 = 300$ K, respectively. In the calculations, we use the formalism discussed in Sec. II, except that we set $E^p_{1\to 2} = E^p_{2\to 1} = 0$ and $R = 0$, i.e., we ignore contributions from phonon-polariton excitations and nonradiative recombination.

We perform these exact calculations for both the homojunction and heterojunction structures. In the homojunction case, we choose InAs as the semiconductor for both bodies. On the hot side (body 2), we set $t_2 = 4$ μm to ensure that it has significant absorption for our wavelengths of operation. On the cold side (body 1), we choose a thickness to be $t_1 = 1$ μm to facilitate the comparison with the nonideal case as discussed in the next section. In the heterojunction case, we choose InSb for the hot body and InAs for the cold body. In our calculations, the data for $\epsilon_e(\omega,0)$ and $\epsilon_p(\omega)$ for InAs and InSb are obtained from [37,44] and [36,45], respectively. Equation (2) is then used to determine the appropriate above-band-gap dielectric function in Eq. (4) when a nonzero voltage is applied. In Eq. (6), we choose $\hbar\omega_c = 0.31$ eV, below which the contribution to photoemission from interband processes for InAs is negligible.

We consider the homojunction case first. Figure 2(a) shows the net outflow power density P_{ideal} as a function of the external bias V for various gap separations d. For every d at $V = 0$, there is net power flow from the hot body (body 2) to the cold body (body 1) and $P < 0$, as expected. As V increases, the outflow from body 1 also increases. As V increases beyond a threshold voltage V_t, P becomes positive and body 1 experiences a net outflow of energy and hence cooling. For this system, Eq. (21) gives a V_t of 0.0122 V, which agrees quite well with the $V_t = 0.0129$ V obtained from the exact calculations. At a large V, the net power density P increases approximately exponentially as a function of V, in agreement with Eq. (19). For a fixed V, the power density increases significantly as one reduces d. This effect is typical of near-field heat transfer where the transferred power increases as the separation d between the two bodies decreases [2].

For the homojunction structure, the numerically obtained COP as a function of V is plotted in Fig. 2(c) for several

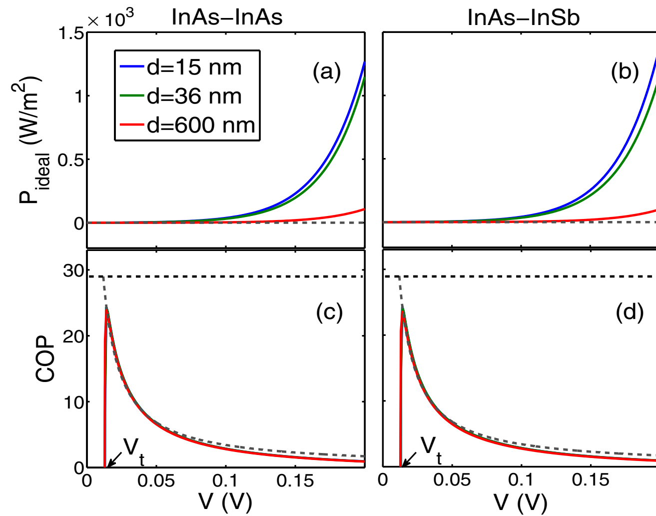

FIG. 2. (Color online) Top row contains plots of P_{ideal} as a function of V of (a) the homojunction and (b) the heterojunction structures for different d (indicated in the legend). The horizontal dashed lines in (a) and (b) represent the zero power densities. Bottom row shows the corresponding COP as a function of V of (c) the homojunction and (d) the heterojunction structures (assuming no nonidealities) for the same values of d as in (a) and (b). The decreasing dashed curves in (c) and (d) are obtained from Eq. (23). The horizontal dashed lines in (c) and (d) represent the Carnot efficiency limit. V_t in (c) and (d) indicates the threshold voltage.

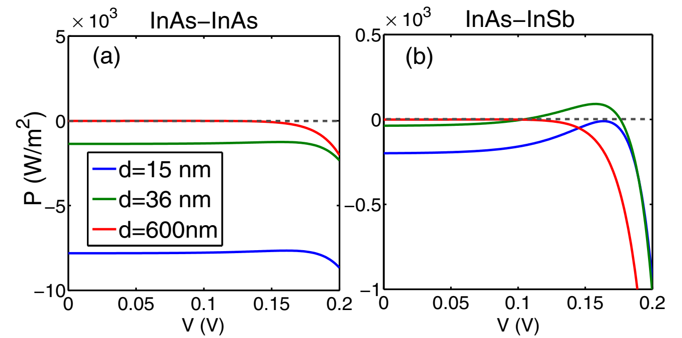

FIG. 3. (Color online) Plots showing P as a function of applied bias V for (a) a homojunction structure consisting of InAs, and (b) a heterojunction structure consisting of InAs and InSb, for different vacuum gap size d. The gray dashed line in (b) indicates the zero power density. Both the effects of Auger recombination and phonon-polariton heat transfer are included.

separations d, and compared to the analytical model of Eq. (23). The analytical model predicts that in the ideal case, the COP should be independent of the separation d as confirmed by the numerical simulations. The only significant deviation from the analytic model occurs near V_t. In particular, the analytic model predicts a discontinuity in COP at V_t, while the exact numerical results show a zero COP at V_t followed by a rapid increase of the COP towards the Carnot limit at a voltage slightly above V_t. The discrepancies here arise since the photon flux rate and the net photon energy transfer rate vanish at slightly different voltages in the exact calculation. This is in contrast to the analytical model where both rates vanish at V_t. As a result, the analytic model becomes inaccurate at V near V_t. The exact numerical results show that our structure can indeed have a cooling performance close to the Carnot limit in the absence of nonidealities.

The numerically obtained power density and COP behaviors for the heterojunction structure are shown in Figs. 2(b) and 2(d), respectively. The behaviors are almost identical to that of the homojunction case, confirming the analysis presented in Sec. III B.

IV. EFFECTS OF NONIDEALITIES

A. Numerical results

In the previous section we showed that in the absence of nonidealities, the configuration shown in Fig. 1 can operate as an ideal cooling device with efficiency approaching the Carnot limit. In this section we consider the effects of the two nonidealities that are intrinsic to the III-V semiconductors used in the configuration of Fig. 1: (1) the Auger recombination process, the dominant nonradiative recombination processes for high-quality material, and (2) phonon-polariton heat transfer, which results in heat flow from the hot body to the cold body that is independent of the electronic transitions and therefore the applied voltage on body 1. The numerical results for the power density P including these two effects are shown in Figs. 3(a) and 3(b) for the homojunction structure and the heterojunction structure, respectively. Unlike the ideal scenario without nonidealities [Figs. 2(a) and 2(b)], where the homojunction structure and the heterojunction structure show identical behaviors, here the two structures behave very differently. For the homojunction case, there is no longer any net cooling for any separation d and at any voltage. For the heterojunction case, there is also no net cooling at the large and small d limits. On the other hand, for the heterogeneous structure with a separation $d = 36$ nm, for example, net cooling can still be achieved with a peak cooling power density of 91.23 W/m^2 at 0.158 V of forward bias on body 1.

In the subsequent sections, we seek to elucidate the effects of nonidealities that lead to the behaviors shown in Fig. 3. We discuss the effects of Auger recombination in Sec. IV B. The combined effects of phonon-polariton heat transfer and Auger recombination are then considered in Sec. IV C. Finally, the performance including both nonidealities is shown in Sec. IV D.

B. Effects of Auger recombination

To illustrate the effect of Auger recombination, we consider the same configurations as shown in Fig. 1 but now with the effect of Auger recombination included. For simplicity, we do not include the contribution from phonon-polariton heat transfer in this section. In the following, we first consider a homogeneous InAs-InAs structure with separation $d =$ 36 nm. Figure 4 plots this example structure's net output power density crossing the vacuum gap as a function of voltage for the cases with and without Auger recombination. We observe from Fig. 4 that for voltages below V_t, the two power density curves almost overlap with one another. This similarity in power

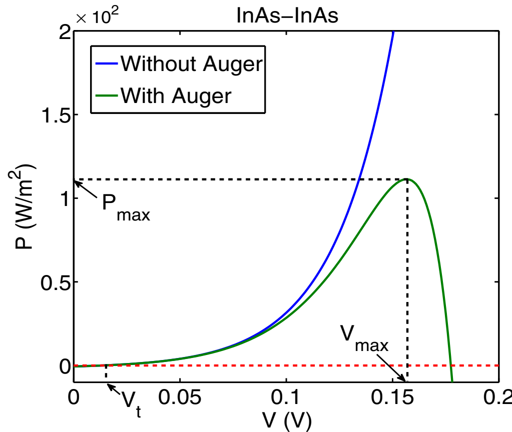

FIG. 4. (Color online) The net outflow power density P as a function of applied voltage V for the cases without (blue curve) and with (green curve) Auger recombination, respectively, for $d = 36$ nm. Phonon-polariton heat transfer is ignored. For the case with Auger recombination, the peak power density is denoted as $P_{\rm max} = 111.31\ {\rm W/m^2}$ with an associate voltage $V_{\rm max} = 0.156$ V. The threshold voltage for body 1 to reach net cooling is labeled $V_{\rm t}$ ($0.013V$), and the zero power density level is denoted by the horizontal dashed red line.

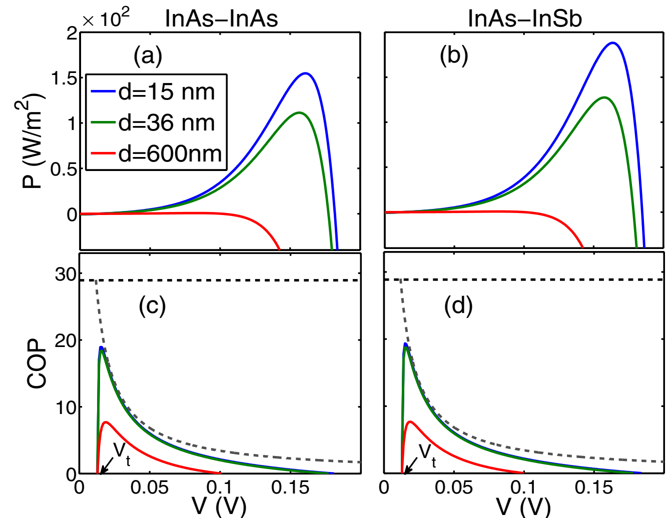

FIG. 5. (Color online) Top row includes plots of power density P as a function of V for (a) the homogeneous and (b) the heterogeneous structures in the presence of Auger recombination. Plots are shown for different separations d [inset of (a)]. (c) and (d) show the COP as a function of V for the same set of d's. The dashed curves in (c) and (d) represent the analytical solution without Auger recombination, as obtained from Eq. (23). The horizontal dashed lines in (c) and (d) represent the Carnot efficiency limit for this configuration.

density is expected since the effect of Auger recombination is sufficiently weak when the applied voltage is small.

However, as V increases beyond $V_{\rm t}$ in Fig. 4, the net outflow power density reaches a maximum for the case with Auger recombination. We can explain this behavior as follows: The semiconductor's carrier density increases significantly as the applied voltage increases beyond $V_{\rm t}$. Furthermore, since the Auger recombination rate in Eq. (12) scales with a higher exponent with respect to carrier density as compared to radiative recombination rate, the nonradiative recombination rate [R in Eq. (11)] increases faster and eventually dominates over the radiative recombination rate. The Auger recombination process generates heat inside body 1. As a result, the net outflow power density from it reaches a maximum as V increases. Therefore in the presence of Auger recombination, there exists an optimal voltage at which the cooling power is maximized.

In Fig. 5, we plot the cooling power density P and the COP as a function of voltage for both homojunction and heterojunction structures with various separations d, taking into account Auger recombination. The homojunction and heterojunction structures show qualitatively similar behaviors. At $d = 600$ nm, there is only small net cooling of approximately $0.76\ {\rm W/m^2}$ for both junctions. Significant cooling is observed for smaller d. For each d, the cooling power density shows a maximum at a specific voltage $V_{\rm max}$, a behavior that was already discussed in Fig. 4 for $d = 36$ nm. Moreover, $V_{\rm max}$ increases as we reduce d. The reduction of d results in an increase of the radiative recombination rate. Hence the system can operate at a higher voltage before the nonradiative recombination process dominates. We also observe an increase of maximum power density as we reduce d. This arises as a result of both the power transfer enhancement for small d, as well as the higher operating voltage.

Figures 5(c) and 5(d) show the COP as a function of applied voltage V for the same separations d in both homojunction and heterojunction structures. In general, the presence of nonradiative recombination reduces the COP. This reduction, however, is far less severe as we decrease the separation d into the near-field region. This is because the nonradiative recombination rate is independent of d, while the radiative recombination rate increases as we reduce d. Thus, the detrimental effect of nonradiative recombination is mitigated as we reduce d.

We also note that such nonradiative recombination is significant only when a forward bias is applied. Hence in these calculations we do not need to include the Auger recombination on the hot side where no voltage is applied. In the heterojunction case, this means that we only need to take into account the Auger recombination on the InAs side. In addition, the Auger combination rate per unit area is proportional to the thickness of the structure, as seen in Eq. (12). Thus for the cold side InAs, we have chosen its thickness $t_1 = 1\ \mu$m as a compromise between the need to maximize emission and the need to reduce Auger recombination.

C. Effects of the phonon-polariton heat transfer

From the discussions above, we see that to mitigate the effect of Auger recombination, one generally prefers to operate in the near-field regime where the separation between the two bodies is small. However, in this near-field regime, the presence of phonon-polariton heat transfer can become very substantial. For a cooling device, such a phonon-polariton heat transfer represents a detrimental leakage pathway.

We plot in Fig. 6 the phonon-polariton contribution to the heat transfer $P_{\rm phonon}$ as a function of gap separation

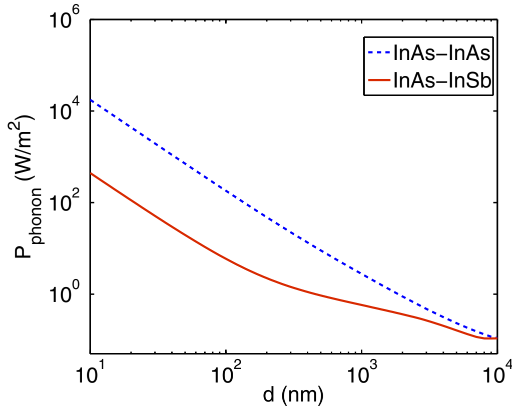

FIG. 6. (Color online) Plot of phonon-polariton heat transfer power density P_{phonon} for the homojunction structure (dashed blue curve) and heterojunction structure (solid red curve) as a function of vacuum gap separation d. At $d = 10$ nm, the phonon-polariton heat transfer in heterojunction structure is one order of magnitude lower than that of the homojunction structure.

d for the homojunction and heterojunction structures. For the homojunction case, the heat transfer power increases approximately as $1/d^2$ when d decreases since the two bodies have surface phonon-polariton excitations with near matching frequencies. This behavior is consistent with the literature on near-field heat transfer [2]. The presence of such strong phonon-polariton heat transfer, in combination with the Auger recombination, is sufficient to eliminate any cooling effect in the homojunction structure, as demonstrated in Fig. 3(a).

To demonstrate cooling in the presence of nonidealities, one therefore needs to mitigate the effect of phonon-polariton heat transfer. As a straightforward approach, we consider a heterojunction structure in which the semiconductors are different. For the heterojunction structure considered in this paper, the surface phonon-polariton excitation frequencies for the InAs-vacuum and InSb-vacuum interfaces no longer match, and hence the phonon-polariton heat transfer is substantially reduced as compared to the homojunction structure (Fig. 6). The use of such heterojunction structures in the near-field regime thus allows us to mitigate the detrimental effects of both Auger recombination and phonon-polariton heat transfer, and therefore enables significant cooling as shown in Fig. 3(b).

D. Performance including both nonidealities

Figure 7(a) shows the peak outflow power density P_{max} as a function of the gap size d for the InAs-InSb structure. At separations $d < 16$ nm, the surface phonon-polariton heat transfer dominates over above-band-gap photon heat transfer and the peak power density is negative, indicating there is a net energy flow from the hot side to cold side and hence the absence of any cooling effect. Whereas for large separations $d > 570$ nm, Auger recombination dominates and we also do not observe any net cooling for body 1. In the intermediate range from 16 to 570 nm, the system can operate as a solid-state cooling device. The largest cooling power density is found when $d = 36$ nm, for which $V = 0.158$ V yields 91.23 W/m^2 of cooling power density against the assumed 10 K temperature difference. In addition, we note that when the two bodies are near thermal equilibrium, the maximum cooling power density in the near field is three orders of magnitude higher than that in the far field.

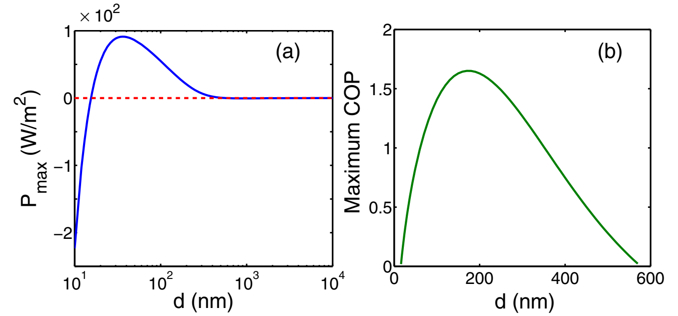

FIG. 7. (Color online) (a) P_{max} versus separation d in the presence of Auger recombination and phonon-polariton heat transfer for the heterojunction structure. (b) The maximum COP as a function of d from 16 to 570 nm for the heterojunction structure.

Figure 7(b) shows the maximum COP achievable for InAs-InSb structures with separations 16 nm $< d <$ 570 nm. The maximum COP is 1.65 and is found at $d = 170$ nm. Such a COP is comparable to that of thermoelectric coolers at similar operating temperatures in practice [46], and is significantly higher than other photon-based solid-state cooling schemes, including laser cooling of solids [47,48]. Therefore, the results here show that the device in Fig. 1 can, in principle, be used as a high-efficiency solid-state cooling device, even in the presence of significant nonradiative recombination and phonon-polariton heat transfer. In addition, by using quantum wells [49] to mitigate Auger recombination and engineering surfaces to reduce the phonon-polariton coupling, higher COP and cooling power density are achievable by our design.

V. CONCLUSION

In summary, in this paper, we have shown that controlling the chemical potential of a thermally emissive body could enable significant new opportunities to exploit near-field electromagnetic heat transfer. These include the capability for electronic control of both the magnitude and the direction of heat flow in nanoscale systems as well as the potential for a solid-state cooling device that operates near the Carnot limit. The cooling effect persists even in the presence of nonidealities such as Auger recombination and phonon-polariton heat transfer. We have further seen that to achieve this, we must place the semiconductor heat absorber in the near field of the electrically driven emitter to mitigate the effect of Auger recombination, and choose a heterojunction configuration that minimized the parasitic phonon-polariton heat transfer in the near field.

ACKNOWLEDGMENTS

This work was supported by the DOE "Light-Material Interactions in Energy Conversion" Energy Frontier Research Center under Grant No. DE-SC0001293.

[1] D. Polder and M. Van Hove, Phys. Rev. B **4**, 3303 (1971).
[2] J. B. Pendry, J. Phys: Condens. Matter **11**, 6621 (1999).
[3] J. J. Loomis and H. J. Maris, Phys. Rev. B **50**, 18517 (1994).
[4] R. S. Ottens, V. Quetschke, S. Wise, A. A. Alemi, R. Lundock, G. Mueller, D. H. Reitze, D. B. Tanner, and B. F. Whiting, Phys. Rev. Lett. **107**, 014301 (2011).
[5] S. Shen, A. Narayanaswamy, and G. Chen, Nano Lett. **9**, 2909 (2009).
[6] E. Rousseau, A. Siria, G. Jourdan, S. Volz, F. Comin, J. Chevrier, and J. J. Greffet, Nat. Photonics **3**, 514 (2009).
[7] A. Kittel, W. Müller-Hirsch, J. Parisi, S. A. Biehs, D. Reddig, and M. Holthaus, Phys. Rev. Lett. **95**, 224301 (2005).
[8] R. St-Gelais, B. Guha, L. Zhu, S. Fan, and M. Lipson, Nano Lett. **14**, 6971 (2014).
[9] A. Narayanaswamy and G. Chen, Appl. Phys. Lett. **82**, 3544 (2003).
[10] C. Luo, A. Narayanaswamy, G. Chen, and J. D. Joannopoulos, Phys. Rev. Lett. **93**, 213905 (2004).
[11] B. Guha, C. R. Otey, C. B. Poitras, S. Fan, and M. Lipson, Nano Lett. **12**, 4546 (2012).
[12] M. Krüger, T. Emig, and M. Kardar, Phys. Rev. Lett. **106**, 210404 (2011).
[13] C. R. Otey and S. Fan, Phys. Rev. B **84**, 245431 (2011).
[14] R. Messina and M. Antezza, Europhys. Lett. **95**, 61002 (2011).
[15] A. Narayanaswamy and G. Chen, Phys. Rev. B **77**, 075125 (2008).
[16] A. W. Rodriguez, M. T. Homer Reid, J. Varela, J. D. Joannopoulos, F. Capasso, and S. G. Johnson, Phys. Rev. Lett. **110**, 014301 (2013).
[17] C. R. Otey, L. Zhu, S. Sandhu, and S. Fan, J. Quant. Spectrosc. Radiat. Transfer **132**, 3 (2014).
[18] A. I. Volokitin and B. N. J. Persson, Rev. Mod. Phys. **79**, 1291 (2007).
[19] C. R. Otey, W. T. Lau, and S. Fan, Phys. Rev. Lett. **104**, 154301 (2010).
[20] L. Zhu, C. R. Otey, and S. Fan, Appl. Phys. Lett. **100**, 044104 (2012).
[21] P. Ben-Abdallah and S.-A. Biehs, Appl. Phys. Lett. **103**, 191907 (2013).
[22] P. Ben-Abdallah and S.-A. Biehs, Phys. Rev. Lett. **112**, 044301 (2014).
[23] P. J. van Zwol, K. Joulain, P. Ben Abdallah, J. J. Greffet, and J. Chevrier, Phys. Rev. B **83**, 201404 (2011).
[24] P. J. van Zwol, L. Ranno, and J. Chevrier, Phys. Rev. Lett. **108**, 234301 (2012).
[25] Y. Yang, S. Basu, and L. Wang, Appl. Phys. Lett. **103**, 163101 (2013).
[26] L. Zhu, C. R. Otey, and S. Fan, Phys. Rev. B **88**, 184301 (2013).
[27] S. Basu and M. Francoeur, Appl. Phys. Lett. **98**, 113106 (2011).
[28] H. Iizuka and S. Fan, J. Appl. Phys. **112**, 024304 (2012).
[29] X. L. Liu and Z. M. Zhang, Appl. Phys. Lett. **104**, 251911 (2014).
[30] P. Würfel, J. Phys. C **15**, 3967 (1982).
[31] C. H. Henry and R. F. Kazarinov, Rev. Mod. Phys. **68**, 801 (1996).
[32] O. Heikkilä, J. Oksanen, and J. Tulkki, J. Appl. Phys. **114**, 223108 (2013).
[33] S. M. Rytov, *Theory of Electric Fluctuations and Thermal Radiation* (Air Force Cambridge Research Center, Bedford, MA, 1959).
[34] P. Berdahl, J. Appl. Phys. **58**, 1369 (1985).
[35] P. Santhanam, D. Huang, R. J. Ram, M. A. Remennyi, and B. A. Matveev, Appl. Phys. Lett. **103**, 183513 (2013).
[36] A. Memon, T. J. Parker, and J. R. Birch, Proc. SPIE **0289**, 20 (1981).
[37] D. E. Aspnes and A. A. Studna, Phys. Rev. B **27**, 985 (1983).
[38] W. C. Chew, *Waves and Fields in Inhomogeneous Media* (IEEE, New York, 1995).
[39] A. W. Rodriguez, M. T. Homer Reid, and S. G. Johnson, Phys. Rev. B **86**, 220302(R) (2012).
[40] O. Heikkilä, J. Oksanen, and J. Tulkki, J. Appl. Phys. **105**, 093119 (2009).
[41] B. L. GeFmont, Z. N. Sokolova, and I. N. Yassievich, Sov. Phys. Semicond. **4**, 592 (1982).
[42] K. L. Vodopyanov, H. Graener, C. C. Phillips, and T. J. Tate, Phys. Rev. B **46**, 13194 (1992).
[43] M. Kardar, *Statistical Physics of Particles* (Cambridge University Press, Cambridge, UK, 2007).
[44] H. R. Philipp and H. Ehrenreich, Phys. Rev. **129**, 1550 (1963).
[45] R. Sanderson, J. Phys. Chem. Solids **26**, 803 (1965).
[46] S. B. Riffat and X. Ma, Int. J. Energy Res. **28**, 753 (2004).
[47] R. I. Epstein, M. I. Buchwald, B. C. Edwards, T. R. Gosnell, and C. E. Mungan, Nature (London) **377**, 500 (1995).
[48] M. Sheik-Bahae and R. Epstein, Laser Photonics Rev. **3**, 67 (2009).
[49] L. Chiu and A. Yariv, IEEE J. Quantum Electron. **18**, 1406 (1982).